EVALUATION OF MULTIPATH EFFECTS ON SAS IMAGERY

J. Ehrlich — Bundeswehr Technical Centre for Ships and Naval Weapons, Maritime Technology and Research (WTD 71), Kiel, Germany
H. Schmaljohann — Bundeswehr Technical Centre for Ships and Naval Weapons, Maritime Technology and Research (WTD 71), Kiel, Germany
W. Jans — Bundeswehr Technical Centre for Ships and Naval Weapons, Maritime Technology and Research (WTD 71), Kiel, Germany

1 INTRODUCTION

In the presence of multipath spreading, which is common in shallow water, sonar imagery is usually disturbed by the contribution of non-direct paths. This holds for conventional side scan sonars as well as for synthetic aperture sonars (SAS). Because SAS imagery is based on data driven motion estimation the limitations resulting from multipath can even be more severe. Therefore, we pre-suppose that the imagery is based on correct motion estimation. This is usually the case if multipath spreading is limited and, thus, only visible for strong scatterers. In this case the contribution of multipath to the image is less dominant for SAS processing because of the extended length of the (synthetic) aperture and the different positions of transmit.
The examined sea data for our study have been gathered with the Atlas Elektronik SeaOtter MKII AUV operated by WTD 71 and equipped with a triple frequency SAS system VISION1200 [1]. This system is described briefly in Chapter 2. The considered data example showing multipath on SAS imagery is presented in Chapter 3. It concentrates on the two lower frequencies (LF, MF) of the used AUV sonar, which illuminate the same patch of seafloor during the same track. For comparison the modelling software MSM was used, which was developed by D. Kraus from the University of Applied Science Bremen and E. Krömer from Atlas Elektronik [2]. This model is briefly introduced in Chapter 4. Simulated amplitudes of multipath propagation are shown in Chapter 4, for a conventional as well as a SAS configuration for both chosen bands and, in addition, compared to the given measured example. Chapter 5 sums up the results and gives an outlook.

2 SEAOTTER MK II AUV OF WTD 71 WITH THE TRIPLE FREQUENCY SAS DEMONSTRATOR

The measurements shown in Chapter 3 were carried out with the SeaOtter MK II AUV of WTD 71 equipped with a new triple frequency VISION1200 SAS system. They were executed in Novembre 2014 during the sonar acceptance tests and took place in the Eckernförde bay in an existing “mine garden” of WTD 71 containing several cylindrical and other object shapes.
The original dual-frequency SAS system VISION1200 developed by ATLAS ELEKTRONIK with a MF and HF center frequencies of $f_{c,\mathrm{MF}} = 75$ kHz, $f_{c,\mathrm{HF}} = 150$ kHz, respectively, had been extended before these tests with a third $f_{c,LF} = 20$ kHz LF transmitter for research purposes. The modified sonar mounted on the SeaOtter Mk II AUV is visible in Fig. 1. The third, much lower, LF frequency band has been chosen for reasons of acoustic penetration into both object and sea bottom (for buried mines). Raw data from this system have been processed by the online SAS processor on board the AUV SeaOtter MK II as well as offline with SAS algorithms originally based on the code by M. Pinto and A. Belletini from NURC [3]. The latter was utilized for this paper. Possibly required adaptions due to, e.g., a much wider SAS aperture for the LF band or beam pattern variations within the LF band [4] have not been included here, because of expected minor impact on the images for this sonar configuration.

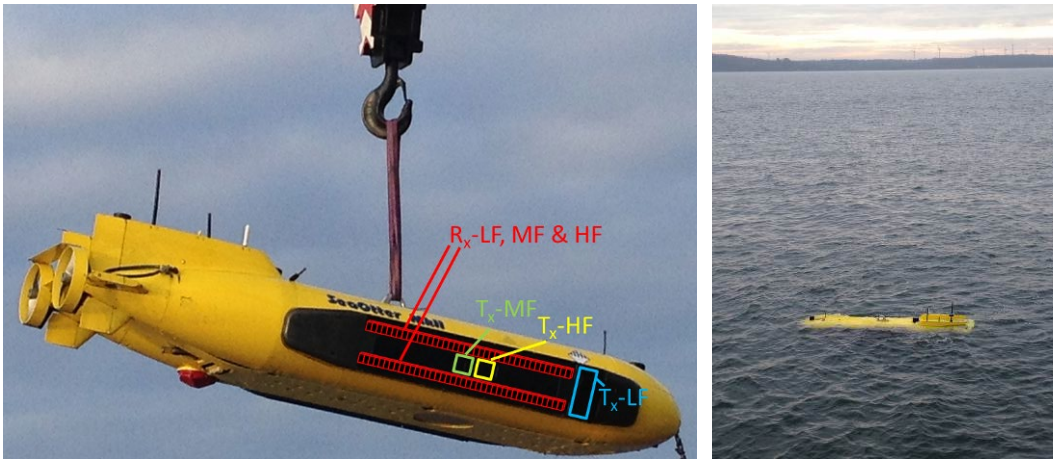

Fig. 1*: SeaOtter MKII equipped with the dual-sided dual-frequency interferometric synthetic aperture sonar VISION1200 extended with a third low frequency transmitter.*

3 MEASURED MULTIPATH RESULTS

The presented measurements in this paper took place in fall 2014 in the Eckernförde bay in an existing “mine garden” of WTD 71 as mentioned previously. During its mission the AUV was operating at a depth of approximately 12 m with 5 m height over ground. The presence of multipath spreading was very likely at this day because of the wind speed of 10 kts (direction: east) and sea state 1 resulting to a flat sea without any waves. During the mission the sonar was transmitting in the LF and MF frequency ranges (almost) simultaneously. Thus, the LF and MF data are conducted under the same environmental conditions. The chosen object of opportunity was lying in a range without multipath influence. This can be derived from the DPCA coherence and leads to a focused SAS image of the object. The LF and MF SAS images of the object are shown in Fig. 2. The cylindrical object was lying at a range of 22.7 m. For the direct path a distinct second highlight

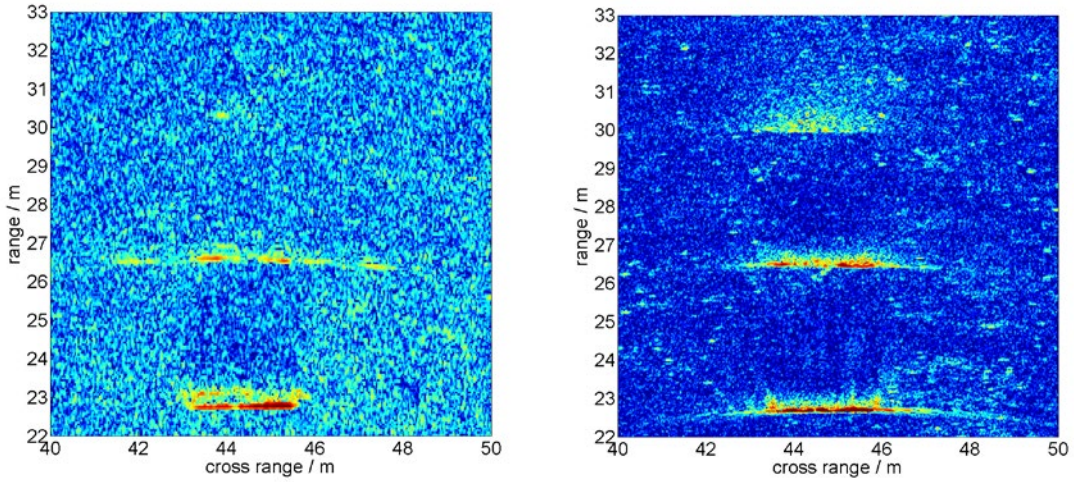

Fig. 2: Two SAS images of the same object of opportunity. The left image is determined using the LF sonar signal and the right image is calculated based on the MF sonar signal. For both images the colour code covers a range of 40 dB.

is observed in the LF image probably indicating an additional reflection at the backside of the object. In both images an additional highlight is visible at a range of 26.5 m. This range corresponds to the first multipath taking the bathymetry and depth of the sonar into account. Finally, the following multi-path at a range of 30 m is clearly present in the MF-SAS image whereas it is only remotely visible in the LF-SAS image.
In the following, we are focusing on the details of the first multipath. For both frequency ranges the shape of the highlight differs from the shape of the direct path. This is expected and caused by the synthetic aperture. The coherent processing does not focus on objects shifted in range by multipath effects. Instead an interference pattern should become visible in the images caused by the uncompensated range errors. For both frequency regimes the intensity drops in the middle of the images of the first multipath of the object. This effect is even more present in the LF-SAS image which is expected because of the wider opening angle for the LF-transmitter. Here, also more highlights can be observed even at higher/lower cross ranges resulting from the longer synthetic aperture. It is assumed that the second multipath is not clearly visible in the LF-SAS image because of the reduced signal to noise ratio in contrast to the MF signal.

4 MSM MODELLING SSS/SAS IMAGERY

4.1 Modelling software MSM

The sonar measurements were modelled with a numerical model based on a ray-tracing formalism. The modelling software MSM, which stands for mine-hunting simulation model, was developed by D. Kraus from the University of Applied Science Bremen and E. Krömer from Atlas Elektronik for the design and analysis of mine-hunting sonar systems [2]. For ray tracing MSM uses an approach based on the dynamic ray tracing formalism developed by Cerveny [5] which gives better results for the pressure amplitude calculations than a standard formulation. MSM is a two-dimensional model working in the frequency space, but it incorporates bandwidth effects to some extent.
The MSM code has a modular design that allows the incorporation of different sub-models for the simulation of the properties of the water (sound speed and absorption) and especially the interaction with the seafloor and the sea surface. The main model for both seafloor and sea surface scattering is a model published by the Applied Physics Laboratory of the University of Washington, usually known as APL-UW model [6]. This model is based on physical assumptions for the interaction of sound with the seafloor and the surface and is widely accepted as a reliable approximation for high frequencies.
A special focus of the MSM code lies on the reverberation calculation with the inclusion of bistatic reverberation. The model traces all paths up to the order of several reflections from sea surface and bottom and uses the paths for the evaluation of the bistatic scattering. For the calculation of the bistatic scattering strength the bistatic scattering model of Ellis and Crowe [7] is used. This model proposes an analytic function for the three-dimensional backscattering which has to be fitted to known results for angles where information exists. The parameters Lambert constant, facet strength and facet slope for the bistatic case are fitted with the results for the monostatic case calculated with the APL-UW model.
Both the conventional sidescan processing and the SAS processing were modelled. For the former the calculations were made with the physical aperture and a sector-beam with a horizontal beamwidth of 30° for the MF transmitter and 37° for the LF transmitter (centre frequency), for the SAS processing the synthetic SAS beam with a constant width of 2 cm independently of range was assumed.
The seafloor and surface reverberation was modelled with the standard ray-tracing formalism that fills space with rays and collects the backscattered energy from bottom and sea surface ordered by reflection history. The returns from the assumed target, a cylinder lying parallel to the path of the AUV, were modelled with an eigenray-tracing mode of the software. The target was discretised with small rectangular facets with the length of the range resolution of the sonar after pulse compression (2.5 cm for MF and 5 cm for LF) and the width of the cross-track resolution (2 cm for SAS-processing and length of the cylinder for the sidescan processing). For all facets that were reached by the sonar all combinations of eigenrays were evaluated and the respective strength of the

resulting combination were collected and added according to their arrival time. The strength of the different arrivals was determined by the losses of the respective paths due to reflections at the bottom and the surface and by the scattering strength at the facet. The former is given by the eigenray calculation, for the latter the scattering from a surface can be approximated with a Kirchhoff scattering approach. For a rectangular plate an analytical formulation can be found that gives the scattering strength based on the geometry of the plate, the scattered and the incident angles and the reflection coefficient [8]. The reflection coefficient was approximated by a calculation with infinite layered plates with concrete on backside, 8 mm of steel for the hull of the cylinder and water on the incident side, according to the formalism of Brekhovskikh [9]. This gives the scattering strength for each facet depending on the angles of incidence and scattering.
In order to compare the simulated levels for reverberation and signal with measurement values a statistical representation has to be generated from the calculated values. Therefore a time series with a Gaussian distribution was created with a variance that corresponds to $\sigma^2 = 1/B \;\; 10^{0.1\,L}$ with L being the level of bottom and surface backscattering and *B* the sonar bandwidth.
The modelling was made at the centre frequencies of the MF- and the LF-band as a representation for the whole band. Looking at the large bandwidth the transducers use this is certainly a simplification and improvements can possibly be made by using a model that takes the different antenna patterns over the bandwidth into account.

For the modelling the section shown in Fig. 2 with the multipath structure was selected. This multipath structure can also be seen in the sidescan processing of the measurements. For the comparison with the modelling an average over six pings covering the target was taken for the sidescan data and an average over the length of the mine for the SAS data. These data will be compared with the simulation of one ping for the sidescan processing and one processed beam for the SAS processing.

4.2 Modelling sidescan processing

The measured return at the position adjacent to the target, averaged over six pings, is depicted versus range in Fig. 3 on the left hand side. On the right hand side the simulated return with a mine-like target placed at the range of 22.5 m from the sonar is shown.

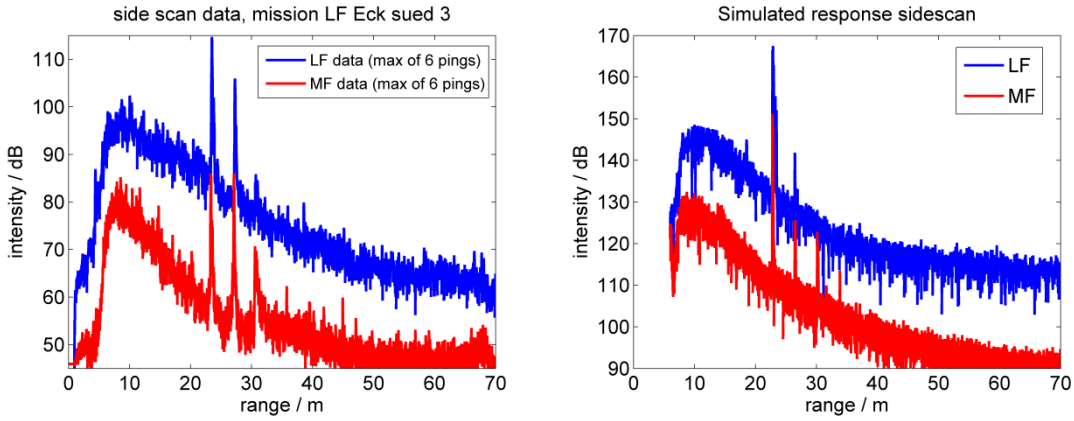

Fig. 3:Left: Sidescan-processed data from the region where the target lies versus range, average of six consecutive pings, Right: Simulated data of one ping in front of the target.

Apart from an offset in the overall levels of approximately 50 dB that has to be explained with signal conditioning and unknown amplifier settings in the sonar recording and processing the shapes of the curves are similar. The decrease of receive level with range is caused by the increasing transmission loss. The observed increase at large ranges in the MF data is possibly caused by a sidelobe in the transmit pattern or sloping bottom in that distance.

The measured data show a strong first multipath return at approximately 27 m after the direct return at 22.5 m, both in MF and in LF. The results for the range between 22 m and 40 m are enlarged in Fig. 4, again showing the measured data on the left hand side and the simulated data at the right.

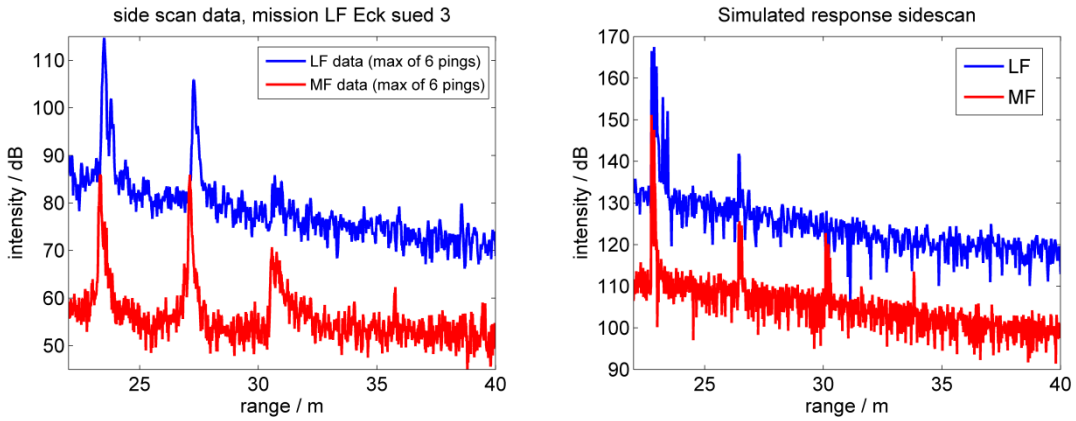

Fig. 4:Left: Close-up of the sidescan-processed data around the target (Fig. 3), Right: Close-up of the corresponding simulated sidescan data

The simulation also produces the main peak from the direct return and the successive peaks from the following multipath returns. However, it fails to explain the strength of the first multipath return, which can be attributed to a sum over paths with one surface reflection. The relative strength of the returns from the facets that add to the first and second peak are shown in Fig. 5.

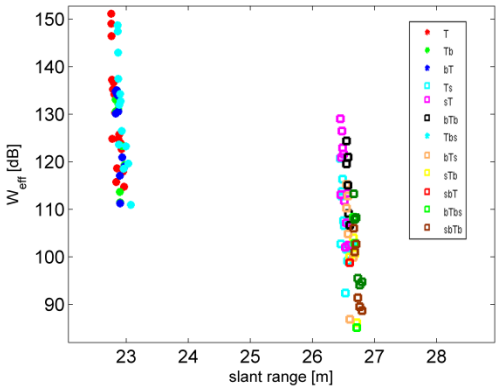

Fig. 5: Effective strength of the individual returns from the facets producing the first peak (direct return) and the second peak (first multipath) in the simulation of the MF signals. The returns are labelled with the letters 'b' for a bottom bounce, 'T' for the reflection from target and 's' for a surface bounce.

The double-peak structure of the direct return can also be reproduced by adding the backside of the cylinder as possible target for the LF simulation, albeit with a reduction of 15 dB for the scattering strength in order to simulate the energy reduction for penetration of the cylinder wall. In general the peaks are broader in the data than in the simulation due to inhomogeneities in the environment.

The calculated levels of reverberation from the seafloor, the sea surface, volume reverberation and ambient noise, compared to the target returns are shown in Fig. 6.

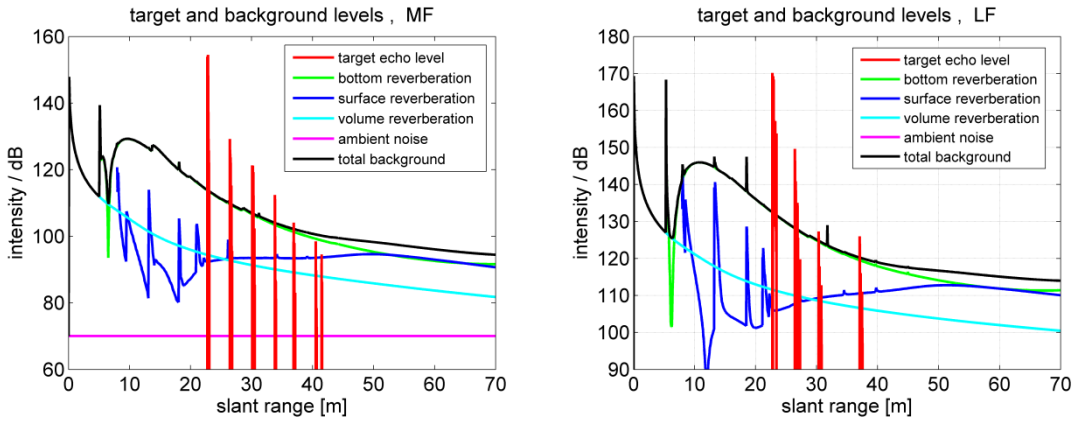

Fig. 6:Levels of target returns (red) and reverberation and noise from the simulation, left: medium frequency sonar, right: low frequency sonar.

4.3 Modelling SAS processing

The modelling of the synthetic aperture sonar processing poses additional problems. Due to the virtual antenna of controllable length the horizontal beam is very narrow compared to the sidescan processing where the physical dimension of the antenna specifies the beam. For the processing a horizontal (cross-range) beamwidth of 2 cm independent of range was chosen. This means that with increasing range a growing number of pings have to be added up in order to achieve the constant cross-track resolution. This leads to an increase in intensity with range which counters the decreasing intensity due to the growing transmission loss. The SAS-processed data for the vicinity of the mine show that the levels of the bottom return remain approximately flat over range, with an increase in the MF signals for large ranges (Fig. 7, left). In the simulation this can be reproduced partly, although not completely (Fig. 7, right).

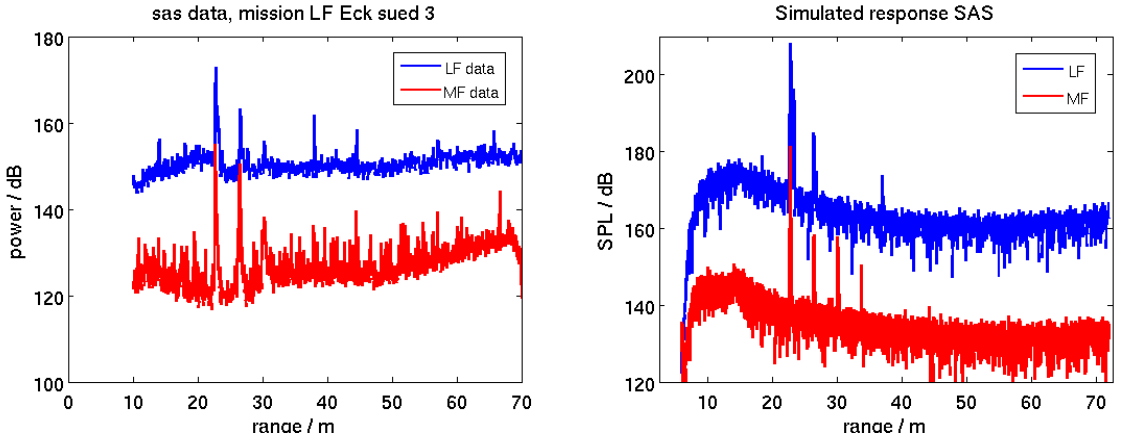

Fig. 7:Left: SAS-processed data from the region where the target lies versus range, average over size of the object, Right: Simulated data of the SAS results in front of the target.

In order to model the SAS-processing a correction factor for the processed intensity level of 20 *$\log_{10}(N*r)$ was introduced. The range r in the correction term is introduced by the synthetic aperture beamforming algorithm used. N is the number of pings added depending on range and is given by $N = L_{SA} * prf / v_{AUV}$ with the length of the synthetic aperture antenna L_{SA}, the pulse repetition frequency prf of the sonar and the speed of the AUV v_{AUV}. The required length of the synthetic aperture is given by the desired cross-range resolution dr, the wavelength λ and the

intended range r as $L_{SA} = \lambda/2\ dr\ * r$. With this correction the SAS-processed levels for the bottom that are fairly independent of range, although a peak in the region between 10 m and 20 m remains. The rise of the level in the measured MF results starting from 50 m is tentatively attributed to coherent noise components present in the signals and a sidelobe in the transmitter pattern.

Also, the simulation tends to overestimate the strength of the first peak, which can be seen in the enlargements of Fig. 8. Processing losses of the SAS processing due to incomplete motion compensation and inhomogeneities along the path of the AUV have not been included correctly.

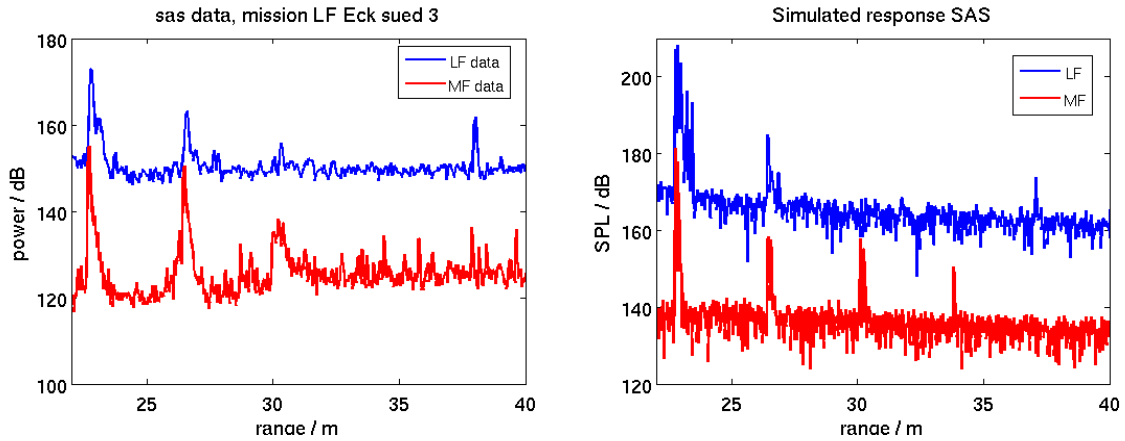

Fig. 8:Left: Close-up of the SAS-processed data around the target (Fig. 7), Right: Close-up of the corresponding simulated SAS data

The sonar data showed that the coherence of successive pings, required for meaningful SAS processing, brakes down at very low ranges shortly after 20 m for MF-sonar signals. This leads to the conclusion that the angles used for the sonars were not set to sensible values for SAS measurements under the prevailing environmental conditions. But one has to bear in mind that the measurements were mostly engineering trials and that the AUV has a third high-frequency transmitter that is meant for the large ranges. This transmitter was not used during the trials. Usually the coherence breaks down if the power of the multipath returns gets larger or at least comparable to the power in the direct return form the seafloor. The strength of these return paths has also been investigated with simulation. The results, shown in Fig. 9, confirm this assumption with the multipath returns from the seafloor dominating over 25 m for MF sonar.

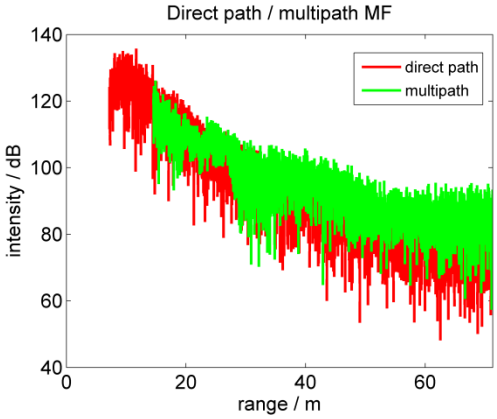

Fig. 9: Modelled returns from the seafloor without target for MF, comparison of the direct return (red) with the summed multipath contributions (green).

5 SUMMARY AND OUTLOOK

Measurements with the SeaOtter MkII AUV with the Vision 1200 synthetic aperture sonar with simultaneous transmission of the LF and the MF sonar have been presented. The measurements revealed strong multipath returns from objects on the seafloor. With an example of a mine-like object lying perpendicular to the path of the AUV the results of these measurements were simulated using the MSM ray-tracing sonar model. Both classic sidescan processing and SAS-processing were modelled. The general multipath structure could be reproduced in the simulation but the high levels of the multipath returns could not be explained completely. Improvements in the modelling can possibly be made in the future if the modelling uses the accurate beampatterns of the sonars and takes the high bandwidth of the signals into account.

6 REFERENCES

1. J. Groen, H. Schmaljohann, S. Leier, W. Jans, Synthetic aperture sonar fusion for images with dissimilar physical content due to differences in acoustic frequency, In proceedings of the 3rd Underwater Acoustics Conference, pp 121-128, Greece, 2015.
2. J. Ehrlich, Calculations for scenario A1 with the MSM code, Proc. IOA, Vol. 32. Pt 2. 2010
3. M. Pinto and A. Bellettini, Design and Experimental Results of a 300-kHz Synthetic Apüerture Sonar Optimized for Shallow-Water Operation, IEEE JOURNAL OF OCEANIC ENGINEERING, pp 285-293, VOL. 34, NO. 3, JULY 2009
4. S. Synnes, R. Hansen, Ultra Wideband SAS-Imaging, in: proceedings of the 1st Underwater Acoustics Conference, pp 111-118, Greece, 2013.
5. V. Cerveny, Ray tracing algorithms in three-dimensional laterally varying layered structures, in *Seismic Tomography*, ed. G. Nolet, Reidel, Boston, 1987.
6. APL-UW High-Frequency Ocean Environmental Acoustic Models Handbook, APL-UW TR9407, AEAS 9501 October 1994, Applied Physics Laboratory, University of Washington, Seattle, Washington 98105-6698;
7. D.D. Ellis, D.V. Crowe, Bistatic reverberation calculations using a three-dimensional scattering function, J. Acoust. Soc.Am., Vol. 89, 2207-2214, 1991
8. B. Nolte, I. Schäfer, J. Ehrlich, M. Ochmann, R. Burgschweiger, S. Marburg, Numerical Methods for wave scattering phenomena by means of different boundary integral formulations, J. Comp. Acous. 15, 495, 2007
9. L.M. Brekhovskikh, Waves in Layered Media, Academic Press, New York, 1980